Desalination and Water Treatment
www.deswater.com

doi: 10.5004/dwt.2017.20317

65 (2017) 11–21
February

Surface modification of TFC FO membrane using *N*-isopropylacrylamide (NIPAM) to enhance fouling resistance and cleaning efficiency

Byung-Moon Jun, Thi Phuong Nga Nguyen, Yu-Kyung Kim, Hyung Kae Lee, Young-Nam Kwon*

School of Urban and Environmental Engineering, Ulsan National Institute of Science and Technology, Ulsan 689-798, Korea, Tel. +(82)52-217-2810; email: kwonyn@unist.ac.kr (Y.-N. Kwon)

Received 1 June 2016; Accepted 29 October 2016

ABSTRACT

Poly(*N*-isopropylacrylamide) (PNIPAM) was grafted onto the surface of commercially available thin film composite (TFC) forward osmosis (FO) membranes via radical graft polymerization at alkaline conditions to improve organic fouling resistance and cleaning efficiency. The successful grafting of PNIPAM to TFC membranes was confirmed using attenuated total reflectance–Fourier transform infrared spectroscopy and X-ray photoelectron spectroscopy, and the grating time for the modification of membrane surface was optimized by monitoring and evaluating peak intensities of the spectroscopies. PNIPAM-grafted membranes exhibited improved resistance to organic fouling compared with the neat membranes when exposed to a synthetic wastewater containing high concentration of alginate foulants. Furthermore, PNIPAM-grafted membrane showed higher cleaning efficiency resulted from the structure transition of PNIPAM-grafted polymers between 25°C and 50°C cleaning solutions. These results indicate that the application of thermo-responsive polymers to FO membranes can improve fouling resistance and cleaning efficiency during the desalination process.

Keywords: Forward osmosis; Fouling resistance; Cleaning efficiency; Poly(*N*-isopropylacrylamide)

1. Introduction

Reverse osmosis (RO)-based desalination has attracted attention in a wide range of processes such as drinking water treatment and reclamation of industrial wastewater [1–5] due to low capital costs from economical land space requirements, low maintenance, and operational costs savings caused by advances in membrane techniques [6]. Even though RO technology has many benefits in desalination, the application of RO can be limiting due to high energy consumption for the process (mechanical energy use of about 4 kWh m^{-3} [7]), and high fouling potential [8]. Recently, hybrid membrane systems including forward osmosis (FO) process have been considered as an alternative desalination method due to its lower energy requirement, fouling potential, and scaling problems compared with conventional RO desalination [9–12]. High hydraulic pressure is not required to operate the FO process, and thus the FO process has several economic benefits over other membrane technologies and the economic feasibility has been reported in the field of seawater desalination, water purification, wastewater treatment, food concentration, and pharmaceutical production with relatively lower fouling and subsequent easy cleaning step [13–17].

However, FO process still has some drawbacks [18]. These include internal concentration polarization (ICP), reverse diffusion with loss of draw solute, and membrane fouling during the operation as well as the absence of proper draw solutes and FO membranes [19–22]. Some of these drawbacks could be reduced by adopting thin film composite (TFC) structures [13,23,24]. Currently, new material (i.e., nanomaterials [25,26]) can be applied to the support layer of FO membrane to enhance water flux [27]. Even though ICP, reverse diffusion, and loss of draw solute can be improved by the optimization of membrane structure, fouling is an

* Corresponding author.

intrinsic and inevitable issue that reduces the performance of membrane processes. Membrane fouling in the FO process is a multifaceted and complex phenomenon, which is affected by the compounding of several factors such as operation modes (active layer faced to feed solution [FS] mode or draw solution [DS] mode), hydrodynamics, characteristics of membrane surface, solution chemistry of feed water, and DS properties [18,28–31]. Membrane fouling mechanism of FO process is different from pressure-driven membrane processes [31]. Previous researches have reported that the fouling in the FO process is relatively lower than that in pressure-driven membrane process, but the fouling severely limits its FO membrane performance [32].

Several strategies have been used to increase the fouling resistance of FO process using physical and/or chemical methods [33–40]. Boo et al. [34] showed that control of hydrodynamic conditions during the operation is effective in mitigating FO membrane fouling; these included (1) enhanced cross-flow velocity of feed and DS, (2) usage of spacers for turbulence generation, and (3) application of pulsed flow in the feed and DS channels. Romero-Vargas Castrillón et al. [35] functionalized TFC FO membranes with poly(ethylene glycol) diglycidyl ether as a steric and hydrophilic barrier to foulant adsorption, resulting in improved organic fouling resistance. Tiraferri et al. [33] showed that surface tailoring of TFC FO membranes using functionalized hydrophilic silica nanoparticles can reduce membrane fouling in the presence of model organic foulants such as alginate, bovine serum albumin (BSA), and Suwannee river natural organic matter. Strong hydrogen bonding interaction between water molecules and hydrophilic membrane surface was shown to prevent the approach of hydrophobic foulants on membrane surface [41]. Li et al. [39] grafted onto polydopamine modified poly(ether sulfone) using synthesized antifouling polymer derived from hyperbranched polyglycerol to improve the resistance of BSA adsorption as well as microbial growths. Zhang et al. [40] showed that surface coating by polydopamine with poly(vinyl alcohol) improved fouling resistance not only to alginate, but also to alginate with calcium complex solution. In addition, several researches have been reported for FO cleaning method. Blandin et al. [42] showed that the membrane fouled with organic foulants can be successfully cleaned using extended osmotic backwashing, and Valladares Linares et al. [43] proposed the application of air scouring and chemical cleaning (e.g., NaOCl) in FO cleaning step.

Meanwhile, it has been reported that the thermo-responsive polymers (TRP) with low critical solution temperature (LCST) can be used to clean fouled/scaled ultrafiltration or RO membranes [44,45]. The application of TRP for cleaning involved penetration of TRP into the fouling layer, transition of TRP to an insoluble form at above its LCST, weakening or breakage of the fouling layer structure, and then removal of foulants during rinsing process [44]. Likewise, surface coating with TRP improved antifouling property by having a brush-like structure [35] and enabling foulants removal easily from the membrane surface [46]. Cheng et al. [46] grafted poly(*N*-isopropylacrylamide) (PNIPAM) onto RO membrane surface, and investigated the effect of TRP on RO performance.

In this work, we present the modification of commercially available TFC FO membrane and use of *N*-isopropylacrylamide (NIPAM) as a grafting agent to improve both fouling resistance and cleaning efficiency of the membrane. Surface properties related to chemical structure, atomic percent of each element, hydrophilicity, surface morphology of the membranes were thoroughly characterized by using attenuated total reflectance–Fourier transform infrared spectroscopy (ATR–FTIR), X-ray photoelectron spectroscopy (XPS), contact angle, and scanning electron microscopes (SEMs) and atomic force microscopy (AFM), respectively. FO process was carried out using synthetic wastewater including alginate organics to investigate the effects of surface modification of TFC FO membranes using NIPAM on the fouling resistance and cleaning efficiency of the membranes.

2. Materials and methods

2.1. Materials

Commercially available TFC FO membrane was purchased from Hydration Technology Innovations (HTI) (Albany, OR, USA) and used as a representative FO membrane. According to previous study [47], the commercial TFC FO membrane used in this study was expressed in integrally asymmetric 'HTI3' TFC membrane which is comprised of three layers of woven polyester substrate material, polysulfone substrate layer which has finger-like structure and dense polyamide active layer. The membrane specification, provided from the manufacturer, is provided in Table 1. Potassium peroxymonosulfate ($2KHSO_5{\cdot}KHSO_4{\cdot}K_2SO_4$) was purchased from Sigma-Aldrich (St. Louis, MO, USA) for the formation of radicals to initiate the graft polymerization. Sodium hydroxide to adjust proper pH, both sodium chloride (NaCl) and magnesium chloride ($MgCl_2{\cdot}6H_2O$) for DSs were obtained from Samchun Chemicals (Seoul, Korea). NIPAM, a grafting monomer, was purchased from Acros Organics (Loughborough, UK). Sodium alginate was obtained from Sigma-Aldrich and used as a representative organic foulant. Monopotassium phosphate (KH_2PO_4), sodium chloride (NaCl), magnesium sulfate ($MgSO_4{\cdot}7H_2O$), sodium bicarbonate ($NaHCO_3$), calcium chloride ($CaCl_2$), and ammonium chloride (NH_4Cl) were purchased from Sigma-Aldrich for the preparation of synthetic wastewater. Milli-Q water (Millipore, Bukkeruca, MA, USA) was used for FS and DS of FO process.

2.2. Modification of TFC FO membranes

The TFC FO membrane samples were washed with Milli-Q water and then soaked in Milli-Q water for at least

Table 1
Specifications of commercial HTI FO membrane

Membrane	HTI–TFC FO
Manufacturer	Hydration Technology Innovations
Water permeation	20 L m^{-2} h^{-1}
Monovalent ion rejection	<99.3%
Test condition	Feed: DI water; draw: 1 M NaCl in FO mode
Operating pH range	2–12

2 d in order to fully hydrate them. The active layer of the wet membranes was faced up and clamped between stainless steel open frames. An aqueous solution of 0.17 mM potassium peroxymonosulfate and 2 wt% NIPAM were prepared and poured on the active side of the membranes to prevent the reaction of NIPAM with support layer of the membranes. And then the pH of the aqueous solution was adjusted to pH 11 to initiate the graft of PNIPAM on the membrane, since potassium peroxymonosulfate generates radicals at alkaline condition [48]. Graft polymerizations were conducted for 1, 3, and 6 h while purging with dry nitrogen continuously. The PNIPAM-grafted membranes were washed thoroughly with deionized water at least 12 h to remove unreacted monomers and neat polymers. Fig. 1 represents the schematic procedure of TFC FO membrane surface modification with PNIPAM.

2.3. Characterization of membranes

2.3.1. Spectroscopic analysis

ATR–FTIR was employed to analyze the chemical properties of the membrane surface and measured by a Nicolet 6700 spectrometer (Thermo Scientific, Waltham, MA, USA) equipped with a flat plate germanium ATR crystal [49]. OMNIC 8.1 software was used for recording the FTIR spectra, correcting their baselines, normalizing the spectra, and finding the peaks. All membrane samples were vacuum dried for at least 48 h prior to the measurements. Background spectrum of air was collected before measurement of each membrane sample. Membrane samples were scanned over continuously purging with nitrogen gas, and 128 scans of average spectra were measured at wavenumbers from 1,450 to 1,700 cm^{-1} with a resolution of 4 cm^{-1}.

Atomic percentages of each element on the neat and PNIPAM-grafted membrane active layer were measured using an XPS (K Alpha, Thermo Scientific, USA). All membrane samples were vacuum dried for at least 48 h prior to the measurements. The X-ray beam penetrated about 5–10 nm from membrane active layer for analysis of the elemental composition of the membrane surface.

2.3.2. Contact angle measurements

When a water droplet is delivered to a membrane surface which is previously exposed to air, the angle observed between the membrane surface and the water drop is determined by free energies at the air–water (γ_{aw}), air–solid (γ_{as}), and water–solid (γ_{sw}) interfaces, and the relationship follows Young's equation $\gamma_{as} - \gamma_{sw} = \gamma_{aw} \cos\theta_c$. A hydrophobic surface (i.e., $\theta_c > 90°$) becomes less wettable due to the higher free energy of its water–solid interface ($\gamma_{as} - \gamma_{sw} < 0$) compared with a hydrophilic surface ($\gamma_{as} - \gamma_{sw} > 0$ and then $\theta_c < 90°$) [35].

Contact angle of Milli-Q water droplet on neat and PNIPAM-grafted membranes was measured using sessile-drop method. 9 μL of 25°C and 50°C water droplets were placed on the membrane surface, and the profile of the water droplet on the membranes was captured with a digital camera (Sony, Tokyo, Japan). The images were then analyzed with a post-processing image software, ImageJ (National Institute of Health, Bethesda, MD, USA), to identify the water/air and water/membrane interfaces and to measure the angle between the interfaces. Different droplet temperatures (25°C and 50°C) were used to investigate the effect of temperature on structural transition of the TRP layer on membrane surface. To obtain representative contact angles, 18 contact angle measurements were performed on three separately prepared membranes coupons. All membrane samples were vacuum dried for at least 48 h prior to the measurements.

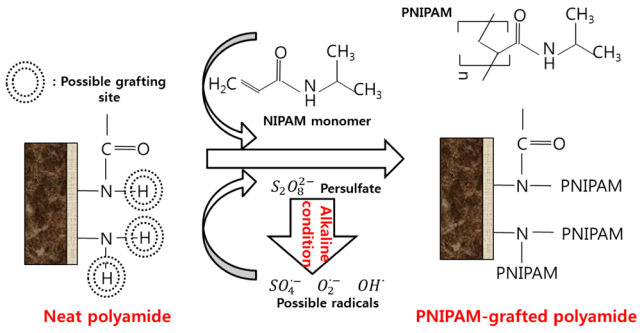

Fig. 1. Schematic illustration of procedure of post-fabrication to graft PNIPAM layer onto TFC FO membrane surface.

2.3.3. Microscopic studies

To investigate membrane morphology of the membranes, top surface images of the membranes were observed using scanning electron microscope (SEM) (Quanta 200, FEI, Hillsboro, OR, USA). All membrane samples were vacuum dried for at least 48 h prior to the measurements. The membrane was rigidly mounted on a specimen by a carbon tape. To reduce image artifacts produced by electrostatic charge, all samples were platinum coated at 20 mA and 2×10^{-3} mbar for 1 min in a turbo pumped high-resolution chromium sputter coater (K575X, Emitech, Lohmar, Germany). Furthermore, surface topography and roughness of the membranes were observed and measured using a Multimode V (Veeco, Santa Barbara, CA, USA) AFM which enables to get the image at vertical lateral resolutions of 0.1 Å. After being dried at vacuum for 48 h, dried membranes were cutted approximately into 1 cm × 1 cm pieces and mounted on a sample stage. Measurement was conducted in tapping mode. Changes of oscillation amplitude of the cantilever as a result of the interactions between the cantilever tip and the sample were recorded, and topography could be obtained by mapping from the target amplitude in voltage [50].

2.3.4. Evaluation of membrane performance

The performance of the FO membranes was investigated in FO mode using the test cells with 27 cm^2 (width: 3 cm and length: 9 cm) effective area [49]. Cross-flow velocity of FS and DS was kept at 28.3 cm s^{-1} using two gear pumps (81808, Cole-Parmer, Vernon Hills, IL, USA), and the performance of neat and PNIPAM-graft membranes was evaluated in terms of water flux and reverse salt flux (RSF) at 25°C ± 1°C. The high cross-flow velocity was applied to minimize external concentration polarization effect during the operation. In addition, various NaCl concentrations from 1.0 to 5.0 M were used to study the effects of DS

concentration on performance with Milli-Q FS. In order to measure the water flux, the DS tank was placed on a digital scale (XP8002S, Mettler Toledo, Billerica, MA, USA) with overhead stirrer, and real-time variation of DS weight was recorded, while FS tank was placed on a magnetic stirrer (Cimarec, Thermo Scientific). The permeate water flux, J_w (L m^{-2} h^{-1}), was calculated by measuring the weight change of DS during 2 h operation after 30 min conditioning for the stabilization of water flux.

$$J_w = \frac{\Delta W}{\Delta t \times A \times \rho} \quad (1)$$

where ΔW (g) is the weight change of the DS over a predetermined time Δt (h), A (m^2) is the effective area of FO membrane, and ρ (g L^{-1}) is the density of the DS.

The RSF, J_s (mole of NaCl m^{-2} h^{-1}), of sodium chloride DS was measured using a calibrated conductivity meter (Thermo Scientific) immersed in FS by converting the conductivity to mole of draw solutes. The reverse solute flux was defined as the mole concentration change of the DSs passing from DS to FS per unit membrane area and unit time.

$$J_S = \frac{\Delta m}{\Delta m \times A} \quad (2)$$

where Δm (mole) is the mole concentration change of the DSs over a predetermined time Δt (h) and the effective FO membrane area A (m^2).

2.4. Evaluation of membrane fouling resistance and cleaning efficiency

Fouling experiments were carried out to investigate alginate fouling of the neat and PNIPAM-grafted membranes under the condition of high organic concentration. Previous studies have shown that alginate foulant causes severe fouling and reduction of water flux in FO membranes [18,28,33,35], and 250 ppm concentration in FS is high enough to accelerate membrane fouling and to observe clearly the organic fouling phenomena occurring on the membrane surface [35]. Therefore, alginate was selected in this study as a model foulant, which represents polysaccharides abundant in wastewater, to investigate the effect of PNIPAM grafting on the fouling resistance. Fouling experiments were conducted with the neat and PNIPAM-grafted membranes in laboratory scale FO test cells described in section 2.3.4. The FS was composed of 250 ppm sodium alginate dissolved in synthetic wastewater solution prepared with $CaCl_2$ (0.50 mM), KH_2PO_4 (0.45 mM), $MgSO_4{\cdot}7H_2O$ (0.61 mM), NaCl (9.2 mM), $NaHCO_3$ (0.50 mM), and NH_4Cl (0.93 mM) at pH ~7.4. Sodium chloride and magnesium chloride were used as draw solute, and the concentration of the DS (from 1.5 to 5 M) was determined to generate same initial permeate water fluxes. Experiments were conducted at a cross-flow velocity of 8.5 cm s^{-1} in both the FS and DS compartments of the flow cell. Each fouling experiment consisted of four parts: baseline test, fouling test, cleaning, and recovery test. Fig. 2 represents the procedures used in this study. First, baseline tests were conducted without an organic foulants in FS which

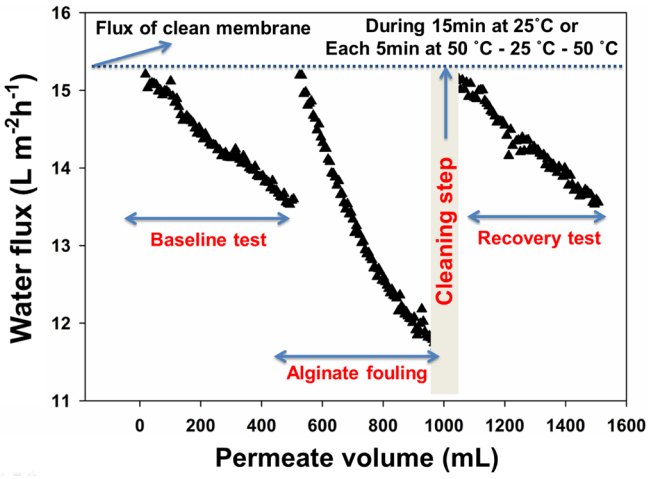

Fig. 2. Procedure of the baseline test, the alginate fouling test, cleaning step, and recovery test used in this study.

contained only the inorganic solutes to measure the extent of flux decline derived exclusively from both DS dilution and reverse draw solute diffusion. In the baseline tests, both neat and PNIPAM-graft membrane have same initial water flux using different concentration ofDS. Second, fouling tests were conducted with 250 ppm alginate in the FS at the same initial flux as the baseline test. The flux decline in fouling test was due to the combined effect of DS dilution and draw solute reverse diffusion as well as membrane organic fouling. Both the baseline and fouling test were conducted until the 500 mL permeate was collected. Shaffer et al. [38] proposed a flux decline value, FD_{500mL}, as a heuristic parameter to evaluate the extent of membrane organic fouling:

$$FD_{500mL} = \frac{\left| \left(\frac{J_{w,f}}{J_{w,0}}\right)_{baseline} - \left(\frac{J_{w,f}}{J_{w,0}}\right)_{fouling} \right|}{\left(\frac{J_{w,f}}{J_{w,0}}\right)_{baseline}} \times 100(\%) \quad (3)$$

where $J_{w,0}$ is the initial water flux and $J_{w,f}$ is the final water flux when 500 mL of permeate accumulated. FD_{500mL} ranges from 0% to 100% where 0% means that there is no difference between flux decline slope at baseline and fouling tests. Likewise, the 100% FD_{500mL} value means no permeate flux due to the complete blockage of water passage. The reason why FD_{500mL} value for evaluating extent of membrane organic fouling is that the FD_{500mL} value can get rid of DS dilution effect on the flux decline, resulting to measure only flux decline by fouling phenomenon.

Third, the fouled membrane was then cleaned physically using Milli-Q water. In this step, Milli-Q water was circulated through the FS and DS compartments for 15 min with cross-flow velocity of 12.5 cm s^{-1} at room temperature (25°C), or alternatively, 15 min cleaning of 5 min at 50°C, 5 min at 25°C, and 5 min at 50°C were conducted in series to study the effect of structure transition of PNIPAM layer on cleaning efficiency. Finally, the recovery of membrane performance after cleaning was investigated. The recovery (%) was calculated

as a heuristic parameter to measure the membrane irreversible fouling.

$$\text{Recovery}(\%) = \left(\frac{J_{w,c,100mL}}{J_{w,0,100mL}} \right) \quad (4)$$

where $J_{w,0,100mL}$ is the average water flux until 100 mL permeate before cleaning and $J_{w,c,100mL}$ is the water flux until 100 mL permeate after cleaning step. Recovery (%) ranges from 0% to 100% where 0% value means that fouling is totally irreversible, and thus there is no flux recovery after membrane cleaning. A recovery value of 100% means that fouling is totally reversible and thus there is complete restoration of water flux after cleaning.

3. Results and discussion

3.1. Characterization of the grafted membrane surface

Surface modification of the commercially available TFC FO membrane was conducted through radical graft polymerization of NIPAM with potassium peroxymonosulfate initiator. The initiator generated radicals such as sulfate radical ($SO_4^{\cdot-}$), superoxide radical ($O_2^{\cdot-}$), and hydroxyl radical ($OH^{\cdot}$) at alkaline conditions [48]. These radicals attacked N–H bond of the aromatic polyamide backbone [51] of the TFC FO membrane [46], thus triggering radical graft polymerization of NIPAM monomer on the membrane surface. Fig. 1 represents schematic illustration of this process. Membrane surface properties related to chemical structure, atomic percent of each element, hydrophilicity, and surface morphology were characterized by ATR–FTIR, XPS, contact angle, and SEM and AFM, respectively. Then, permeation properties of the neat and PNIPAM-grafted membrane were evaluated.

3.1.1. Surface chemistry

ATR–FTIR spectra of neat and PNIPAM-grafted membranes were measured, and the spectra over 1,450–1,700 cm^{-1} are presented in Fig. 3. The penetration depth of the IR beam in the wavenumber region was more than 1 μm, and thus the spectra includes both bands of polyamide skin layer of 100–300 nm thickness and polysulfone support layer [52]. The peaks at around 1,663 and 1,540 cm^{-1} are amide I and II bands resulting from mainly C=O stretching and N–H bending motion of amide bonds, respectively. The other peaks at around 1,586 and 1,487 cm^{-1} are contributed from polysulfone sublayer. The degree of grafting could be evaluated by the intensity ratio of polyamide bands to polysulfone bands [53]. The ratio increased after grafting of PNIPAM showing the enhancements of the amide peaks' intensities after modification. Furthermore, the value of ratio increased monotonically with increasing reaction time from 1 to 6 h. These results suggest that PNIPAM polymer has been successfully grafted onto the TFC FO membrane surface. The optimum condition of PNIPAM for further FO experiment (fouling resistant and cleaning efficiency test) was chosen at 6 h of graft polymerization considering highest degree of PNIPAM grafting (checked by ATR–FTIR peaks).

To confirm the grafting of PNIPAM on TFC FO membrane, XPS analysis was also conducted to characterize the elemental composition of the neat and PNIPAM-grafted membranes. As shown in Fig. 4, atomic percent of carbon/oxygen/nitrogen elements of the neat membrane, PNIPAM-grafted membrane, and NIPAM monomer were 71.4/21.2/7.4, 72.0/19.9/8.1, and 75/12.5/12.5, respectively. The atomic percent value of each element of PNIPAM-grafted membrane was between the values for neat membrane and NIPAM monomer, indicating the successful grafting of the PNIPAM onto the TFC FO membrane surface.

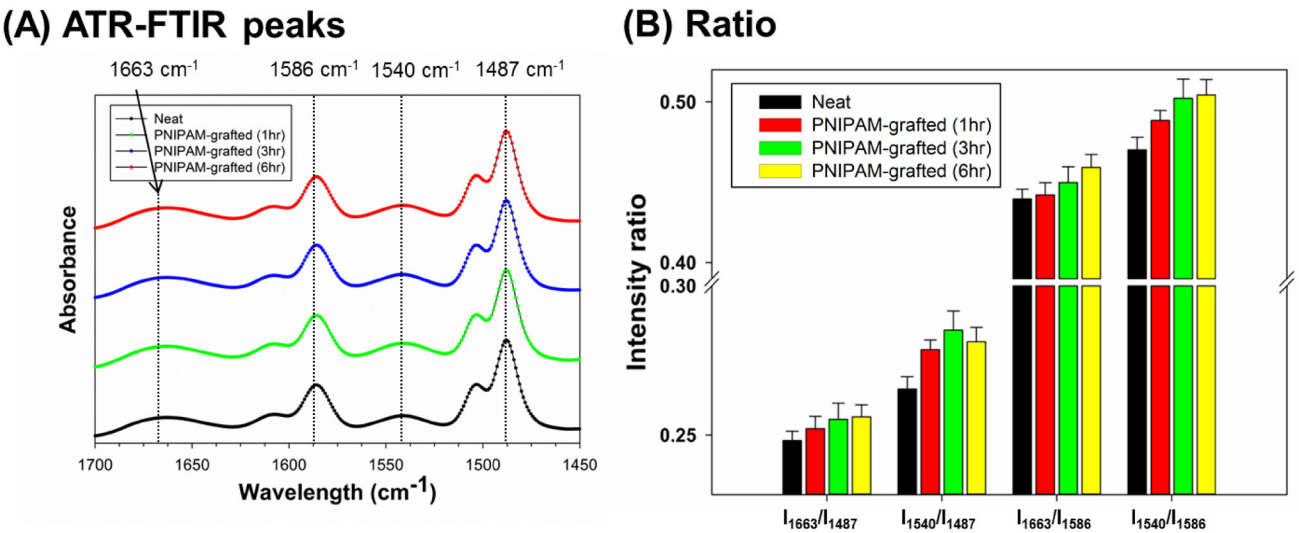

Fig. 3. (A) ATR–FTIR spectra of characteristic bands from 1,400 to 1,800 cm^{-1} related to the membrane polyamide active layer as well as the underlying polysulfone support layer for neat and PNIPAM-grafted membrane with 1, 3, and 6 h reaction time. Absorbance peaks at wavenumbers 1,487 and 1,586 cm^{-1} and 1,540 and 1,663 cm^{-1} are attributed to the membrane polysulfone support layer and polyamide active layer, respectively. (B) Intensity ratio of polyamide active layer and polysulfone support layer to compare degrees of grafting of both neat and PNIPAM-grafted membranes with reaction time.

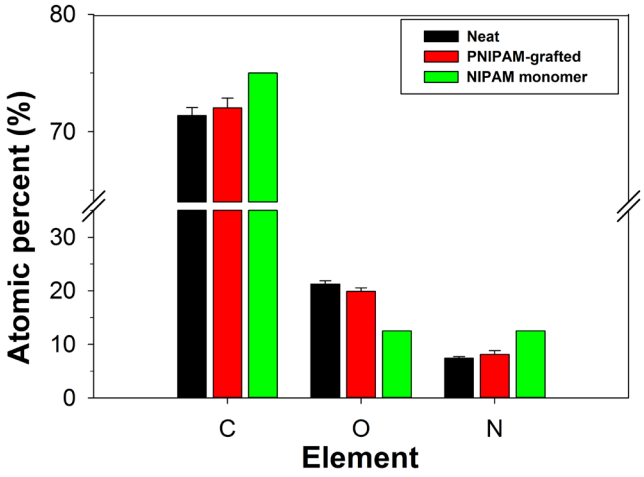

Fig. 4. Characterization of neat and PNIPAM-grafted membrane in terms of elemental composition. Noted that NIPAM monomer as calculated by chemical structure consists of six carbons, one oxygen, and one nitrogen atom.

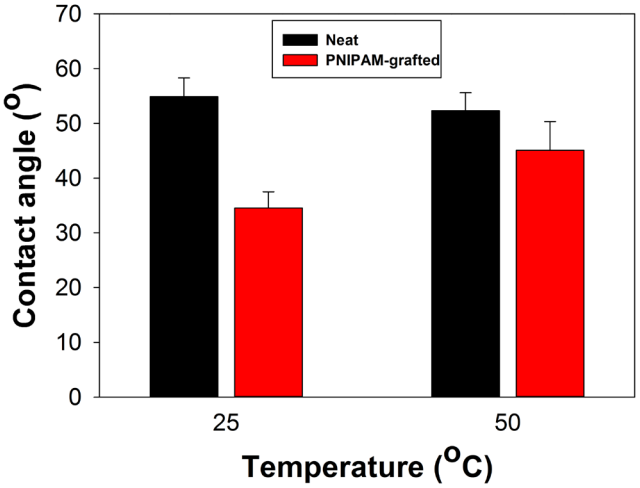

Fig. 5. Comparison of measured water contact angles of neat and PNIPAM-grafted membrane at different solution temperatures (25°C and 50°C).

3.1.2. Contact angle

Change of membrane hydrophilicity due to the surface modification was evaluated by measuring water contact angle. Fig. 5 shows the water contact angles of neat and PNIPAM-grafted membrane at 25°C and 50°C. The surface contact angle of neat membranes at 25°C decreased from 54.9° ± 3.4° to 35.1° ± 2.5° after 6 h of graft polymerization. This result shows that the hydrophilicity of the membrane was improved after grafting with NIPAM [45,46]. It has been reported that hydrophilic membrane causes less organic fouling during the operation [35,36], and thus contact angle measurement can be used as an indicator of fouling resistances of PNIPAM-grafted membrane. The effect of surface modification on fouling was discussed in detail at the next section 3.2. When the droplet temperature increased from 25°C to 50°C, the contact angle of the neat membrane

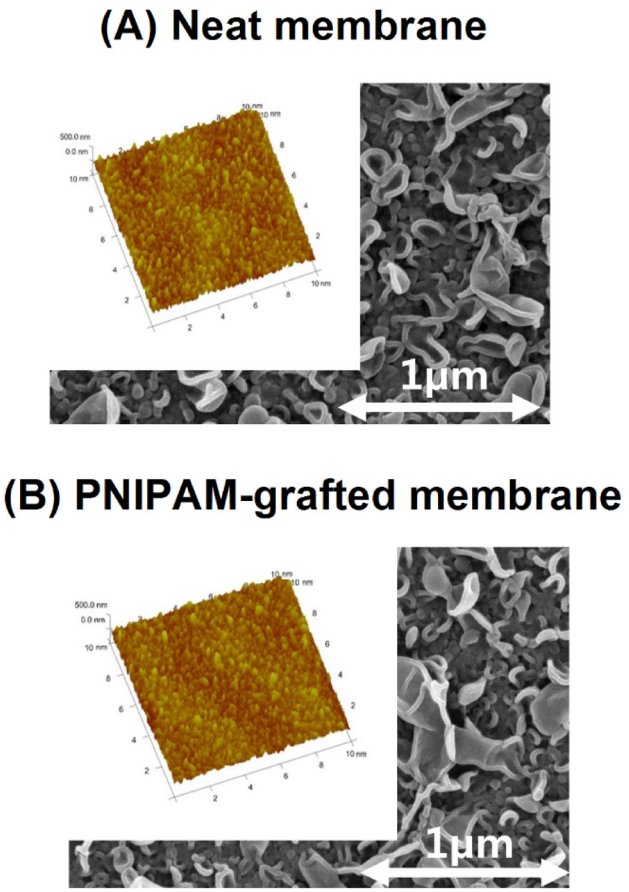

Fig. 6. Surface morphology observed by SEM and AFM for (A) neat membrane and (B) PNIPAM-grafted membrane.

decreased slightly from 54.9° ± 3.4° to 52.3° ± 3.3°. The liquid surface tension decreased with an increase in the temperature [54], and the decrease in water surface tension caused a decrease of the contact angle value [55]. On the other hand, the contact angle of the PNIPAM-grafted membrane showed a reverse tendency. When the droplet temperature changed from 25°C to 50°C, the contact angle value increased from 35.1° ± 2.5° to 45.7° ± 8.7° even though the water surface tension decreased at elevated temperature. This resulted from the structural transition of PNIPAM chains grafted onto the membrane surface when the droplet temperature altered across the LCST of PNIPAM (~32°C) [56]. This transitional characteristic of PNIPAM at environmental temperature was utilized to improve the cleaning efficiency of membrane described in section 3.3.

3.1.3. Membrane morphology

The surface morphological structure of the neat and PNIPAM-grafted membrane was characterized by SEM and AFM images, and is shown in Fig. 6. The surface of neat membrane shows ridge-and-valley structure as general polyamide membrane [57]. However, no significant changes occurred during the grafting of PNIPAM. Roughness of the neat and PNIPAM-grafted membrane was 59.4 ± 1.6 nm and 57.2 ± 0.64 nm, respectively. This result was consistent with

SEM images, and it clearly indicates that the surface modification performed in this study and another similar study [46] did not significantly influence the surface roughness.

3.1.4. Permeation properties in terms of water flux and RSF in FO process

Fig. 7 summarized the permeation properties of the neat and PNIPAM-grafted membrane in FO process. PNIPAM grafting reduced the membrane water flux. The water flux of PNIPAM-grafted membranes gradually decreased with increasing reaction time (from 14.97 ± 0.71 to 11.81 ± 1.40 L m^{-2} h^{-1}), while the hydrophilicity consistently increased with increasing reaction time (Table 2). It seems that the water flux decline was due to the increased resistance to mass transport produced by the grafted PNIPAM layer. Similar reductions in water flux or water permeability have been reported for attachment of other polymer layer such as PNIPAM-*co*-acrylamide [45] and Jeffamine [38] to commercial TFC RO membrane, and other poly(ethylene glycol) derivatives to commercial polyamide NF membranes [58] and to TFC FO membranes [35]. Meanwhile, RSF of the neat and PNIPAM-grafted membrane was not significantly different after grafting. Maintenance of similar RSF value between neat and PNIPAM-grafted membrane indicates that the grafting method (by redox system in this study) did not physically damage the active layer of neat membrane. Again, the optimum condition of PNIPAM for further FO experiment (fouling resistance and cleaning efficiency test) was obtained at 6 h of graft polymerization considering highest degree of PNIPAM grafting.

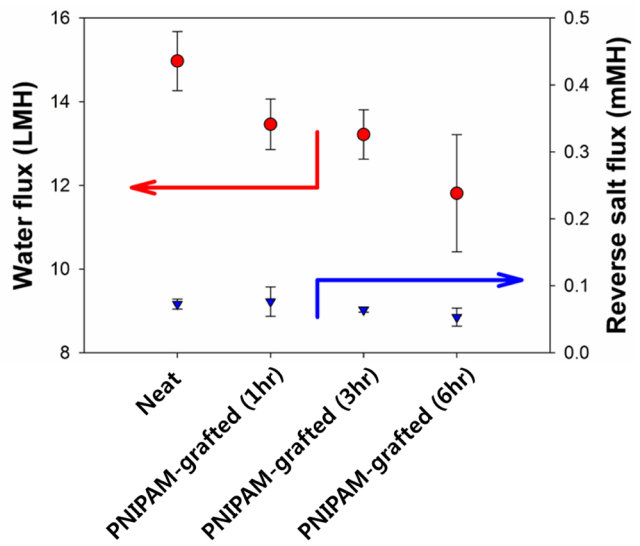

Fig. 7. The permeation properties of the neat and PNIPAM-grafted membrane (1, 3, and 6 h reaction time) in FO process. Conditions: the FS was Milli-Q water and the DS was 1 M NaCl at 25°C temperature. The cross-flow velocity of both sides was 28.3 cm s^{-1} to minimize external concentration polarization (ECP) and the membrane cell was in vertical orientation.

Table 2
Comparison of measured water contact angles of neat and PNIPAM-grafted membrane (1, 3, and 6 h reaction time) at room temperature (25°C)

Membrane	Contact angle (°)
Neat	54.9 ± 3.4
PNIPAM-grafted (1 h)	43.3 ± 2.4
PNIPAM-grafted (3 h)	42.8 ± 1.5
PNIPAM-grafted (6 h)	35.1 ± 2.5

3.2. Fouling resistance of the grafted membrane

Flux decline can occur during the organic fouling experiments with a batch FO system due to both the osmotic pressure decline caused by dilution of DS/concentration of FS and the accumulation of alginate foulants on the membrane surface. The two factors causing the FO flux decline were differentiated by the baseline experiments and fouling tests operated in the absence and presence of organics, respectively. The flux decline (FD_{500mL}) value enabled us to estimate the extent of flux decline caused by only organic fouling during the organic filtration. Fig. 8(A) shows that the flux was considerably reduced in the both neat and PNIPAM-grafted membranes. FD_{500mL} value was calculated in this study as a heuristic parameter to evaluate the extent of organic fouling [38] during 500 mL filtration of FS using Eq. (3). The FD_{500mL} ranges from 0% to 100% where 0% means that there is no observed difference in flux decline at the baseline and fouling tests, implying lower value of FD_{500mL} has higher fouling resistance. Likewise, the 100% FD_{500mL} value means the complete loss of permeate flux during the fouling experiment. Fig. 8(C) presents the FD_{500mL} parameter measured in fouling experiments of neat and PNIPAM-grafted membranes. To ensure the reproducibility of the test, experiments were replicated twice using independently fabricated membranes. When NaCl was used as a DS, the PNIPAM-grafted membranes exhibited 16.7% ± 1.7% FD_{500mL}, which is about 50% enhancement compared with 24.6% ± 2.1% of the neat membranes, demonstrating that the surface modification with TRP improved organic fouling resistance. Meanwhile, the divalent cations such as calcium or magnesium in the simulated wastewater FS might facilitate bridging and complexation between carboxyl groups on the polyamide surface and alginate molecules [59,60]. Divalent ions in the FS can accelerate fouling by mitigating the electrostatic repulsion between foulants and the membrane surface (foulants [61,62] as well as membrane surface [22] were negatively charged at pH 7.4). Complexation by divalent ions increases the formation of an alginate gel layer on the membrane surface, resulting in additional hydraulic resistance for water permeation. Furthermore, the alginate fouling layer might develop cake-enhanced osmotic pressure via the accumulation and trapping of reverse draw solutes in the caked fouling layer, resulting in a decrease of the net osmotic driving force [29]. The monovalent ion such as sodium diffusing from DS to FS can disrupt calcium bridges between foulant molecules in fouling layer as a result of cation exchange [63,64]. The fouling test of neat and PNIPAM-grafted membrane was conducted under the condition of same initial flux. PNIPAM-grafted membrane needed higher DS concentration to generate same initial permeate water fluxes (Fig. 8), resulting higher RSF at higher DS. RSF is proportional to the

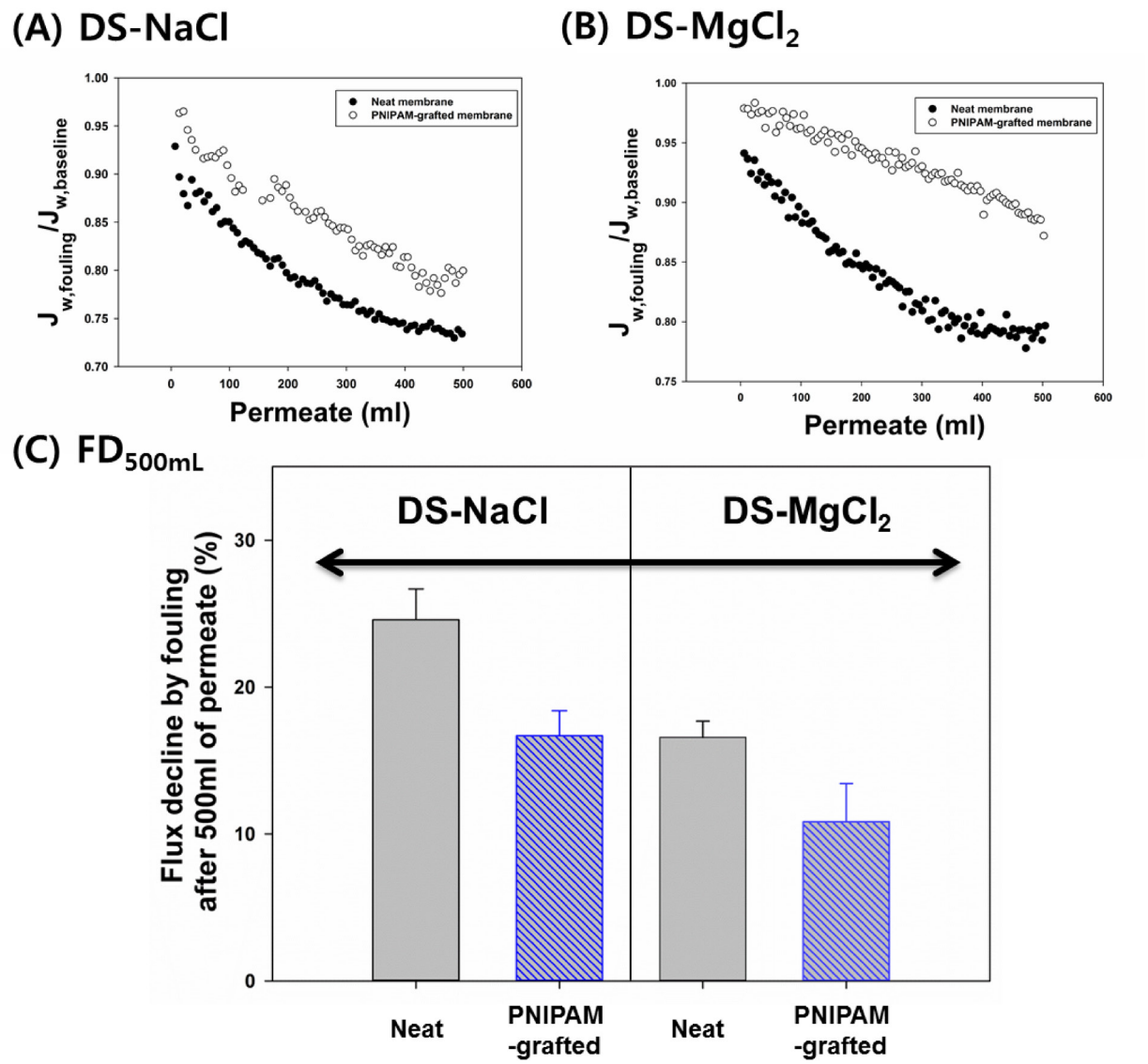

Fig. 8. Comparison of neat and PNIPAM-grafted membrane in terms of permeate flux decline due to organic fouling during 500 mL (A) NaCl as a DS and (B) $MgCl_2$ as a DS. (C) FD_{500mL} values are shown for experiments by organic fouling conducted with NaCl as a DS (initial baseline flux $J_{w,0}$ = 16.0 ± 0.59 L m^{-2} h^{-1}) and $MgCl_2$ as a DS (initial baseline flux $J_{w,0}$ = 14.0 ± 1.2 L m^{-2} h^{-1}), where $J_{w,baseline}$ is the water flux of baseline test and $J_{w,fouling}$ is the water flux of fouling test until 500 mL of permeate volume is accumulated.

concentration difference between FS and DS across the membrane, consequentially, RSF might increase proportionally to the increase of DS concentration (Table 3) [47]. The gel layer weakening, induced by the more breakage of calcium bridge resulted from more pass of sodium at elevated concentration of DS, can cause less fouling of PNIPAM-graft membranes. To assess this possibility, fouling tests were repeated with $MgCl_2$ as the draw solute, which does not have the cation exchange capability compared with NaCl. The fouling behaviors of both neat and PNIPAM-grafted membranes evaluated with $MgCl_2$ DS are presented in Fig. 8(B). Even though there is no influx of the sodium ions from the DS to the foulant layer, the PNIPAM-grafted membrane still showed a lower flux decline (10.84% ± 2.6%) than the neat membrane (16.6% ± 1.1%). Therefore, the lower fouling propensity of the PNIPAM-grafted membrane

Table 3
The permeation properties of the neat membrane at various concentrations of DS from 1 to 4 M

DS concentration	Water flux (L m^{-2} h^{-1})	Reverse salt flux (mole NaCl m^{-2} h^{-1})
1 M NaCl	14.97 ± 0.71	0.073 ± 0.0074
2 M NaCl	19.75 ± 0.27	0.20 ± 0.014
4 M NaCl	24.27 ± 0.34	0.40 ± 0.0089

Note: The DS was NaCl and the FS was Milli-Q water. Active layer of membranes was exposed to the FS. Conditions: the FS was Milli-Q water and the DS was 1 M NaCl at 25°C temperature. The cross-flow velocity of both sides was 28.3 cm s^{-1} to minimize ECP and the membrane cell was in vertical orientation.

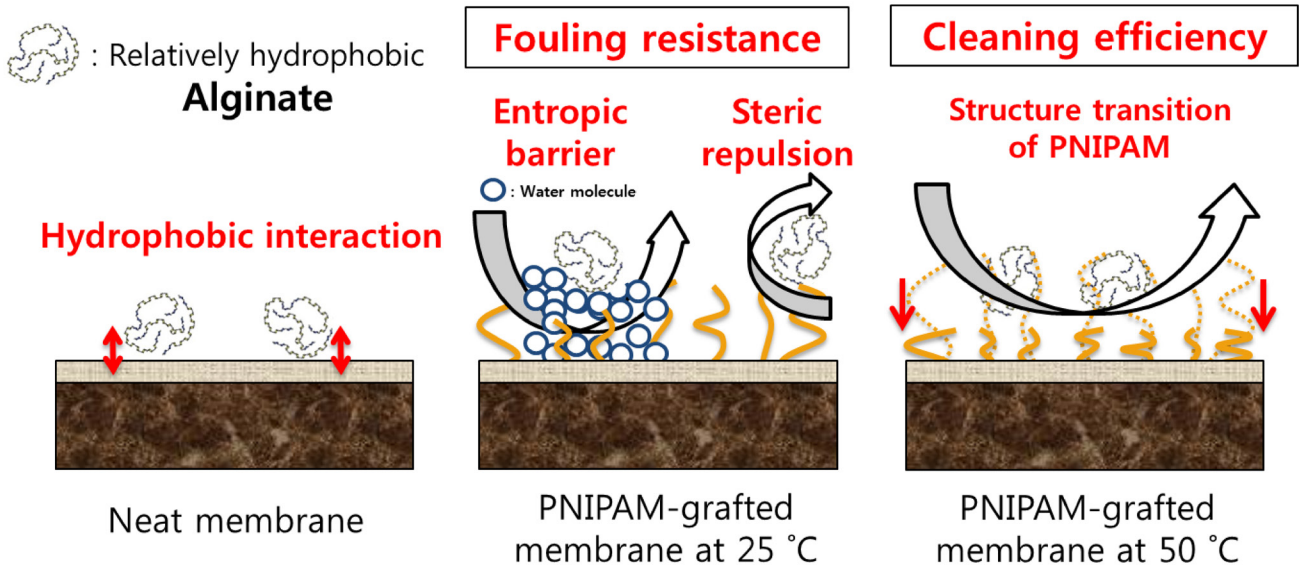

Fig. 9. Schematic illustration of the antifouling mechanisms as well as cleaning efficiency of the PNIPAM-grafted membrane.

was not affected by the disruption of calcium bridging and complexation due to the diffusion of more sodium ions from DS to FS. It seems that the improved organic fouling resistance of the PNIPAM-grafted membranes comes from (1) the strong hydration capability of PNIPAM chains to create water barrier around grafted polymers preventing adsorption of hydrophobic organics (entropic barrier effect [36]) and (2) the steric repulsions effect by the brush-like dangling PNIPAM chains (Fig. 9).

3.3. Recovery test of the grafted membrane after fouling test

The extent of irreversible fouling can be evaluated by recovery measurement of membrane flux after cleaning. Recovery (%) of the neat and PNIPAM-grafted membrane was estimated by calculating the ratio of the initial permeate water flux at baseline test to that at recovery test after membrane cleaning (Table 4). Fouling reversibility is widely known as attribution of the relatively loose structure of the accumulated foulant layer [65]. The loose and sparse layer of foulants (alginate) formed during fouling can be easily separated and removed by physical cleaning with high cross-flow velocity [18]. The recovery (%) after cleaning with Milli-Q water at 12.5 cm s^{-1} cross-flow velocity of both neat and PNIPAM-grafted membranes was more than 80%. The recovery of water fluxes of the PNIPAM-grafted membrane was more than 90%, whereas the recovery of water fluxes of the neat membrane was about 80% regardless of cleaning solution temperature. Furthermore, the PNIPAM-grafted membrane showed a relatively high recovery at lukewarm temperature (50°C) rinsing than at room temperature. The value of recovery (%) was 98.8 ± 1.8 for the PNIPAM-grafted membrane, while it was 82.7 ± 0.77 for the neat membrane. The recovery (%) using cleaning solution of lukewarm temperature enhanced only in the case of PNIPAM-grafted membrane. It is attributed to the structure transition of the grafted PNIPAM-polymer chains when washed with lukewarm water, which releases the foulant layer (alginate) deposited on the membrane surface and thereby assists in the removal of foulants located on the membrane surface [66].

Table 4
Calculated recovery (%) of the fouled both neat and PNIPAM-grafted membrane after cleaning

Cleaning procedure	15 min (25°C)	5 min (25°C) - 5 min (50°C) - 5 min (25°C)
Neat membrane (%)	83.2 ± 5.1	82.7 ± 0.77
PNIPAM-grafted membrane (%)	91.9 ± 5.1	98.8 ± 1.8

The grafting reaction of PNPAM on FO membrane reduced the initial water flux due to the increased resistance across the membrane by the grafted PNIPAM polymer as shown in Fig. 7. However, the surface modification showed good resistance to organic fouling as well as a high recovery (%) after cleaning (Fig. 8) indicating long-term operation may significantly overcome the initial loss of flux. The advantages of this technique involves the improvement of membrane lifetime, reduction of pretreatment process in the presence of organic foulants in feed, and its high potential to the application of co-friendly solar energy, waste heat (low grade heat), and geothermal energy to enable structure transition of PNIPAM layer to clean the fouled membranes.

4. Conclusion

This study has discussed the effect of thermo-responsive dangling PNIPAM polymer grafted via redox system using persulfate at alkaline conditions on organic fouling resistance and cleaning efficiency. ATR–FTIR and XPS spectroscopy supported the successful grafting of PNIPAM layer on commercial TFC FO membrane surface. Contact angle measurement showed the improvement of hydrophilicity at PNIPAM-grafted membrane. Membrane morphology observed by SEM and AFM images was not significantly

different after grafting of PNIPAM layer. The water flux after surface modification reduced as a result of additional resistance to mass transport produced by the grafted PNIPAM layer. However, reverse diffusion of draw solutes in the neat and PNIPAM-grafted membrane was not significantly changed at various grafting times.

In terms of fouling resistance and cleaning efficiency, PNIPAM-grafted membrane showed enhanced fouling resistance due to both entropic barrier and steric repulsion effects. Furthermore, PNIPAM-grafted membrane revealed higher cleaning efficiency by structural transition of PNIPAM chains between 25°C and 50°C of cleaning solution. Post-modification of FO membranes by PNIPAM polymer can be expected to apply in desalination field of various water resources such as wastewater or seawater, because there are several advantages such as (1) its relative easy procedure and (2) its high fouling resistance and cleaning efficiency. For the structure transition, eco-friendly solar energy, waste heat (low grade heat), and geothermal energy can be used. This study suggests that the surface modification of FO membranes with TRP can improve fouling resistance and cleaning efficiency and can be applied to the field of desalination to reduce operation and maintenance costs.

Acknowledgments

This study was supported by the Industrial Fundamental Technology Development Program (10050503) and Korea Institute of Energy Technology Evaluation and Planning (KETEP) through 'Human Resources Program in Energy Technology' (No. 20164030201010) funded by the Ministry of Trade, Industry and Energy, Republic of Korea.

References

[1] Y. Kim, S. Lee, H.K. Shon, S. Hong, Organic fouling mechanisms in forward osmosis membrane process under elevated feed and draw solution temperatures, Desalination, 355 (2015) 169–177.
[2] Y.N. Kwon, C.Y. Tang, J.O. Leckie, Change of membrane performance due to chlorination of crosslinked polyamide membranes, J. Appl. Polym. Sci., 102 (2006) 5895–5902.
[3] H. Choi, J. Park, T. Tak, Y.-N. Kwon, Surface modification of seawater reverse osmosis (SWRO) membrane using methyl methacrylate-hydroxy poly(oxyethylene) methacrylate (MMA-HPOEM) comb-polymer and its performance, Desalination, 291 (2012) 1–7.
[4] S. Hong, I.-C. Kim, T. Tak, Y.-N. Kwon, Interfacially synthesized chlorine-resistant polyimide thin film composite (TFC) reverse osmosis (RO) membranes, Desalination, 309 (2013) 18–26.
[5] Y.-N. Kwon, S. Hong, H. Choi, T. Tak, Surface modification of a polyamide reverse osmosis membrane for chlorine resistance improvement, J. Membr. Sci., 415–416 (2012) 192–198.
[6] M. Pirbazari, B.N. Badriyha, V. Ravindran, MF-PAC for treating contaminated with natural and synthetic organics, J. Am. Water Works Assoc., 84 (1992) 95–103.
[7] G. Raluy, L. Serra, J. Uche, Life cycle assessment of MSF, MED and RO desalination technologies, Energy, 31 (2006) 2361–2372.
[8] M. Herzberg, S. Kang, M. Elimelech, Role of extracellular polymeric substances (EPS) in biofouling of reverse osmosis membranes, Environ. Sci. Technol., 43 (2009) 4393–4398.
[9] M.A. Darwish, H.K. Abdulrahim, A.S. Hassan, A.A. Mabrouk, A.O. Sharif, The forward osmosis and desalination, Desal. Wat. Treat., 57 (2016) 4269–4295.
[10] S. Gormly, J. Herron, M. Flynn, M. Hammoudeh, H. Shaw, Forward osmosis for applications in sustainable energy development, Desal. Wat. Treat., 27 (2011) 327–333.
[11] R.V. Linares, Z. Li, V. Yangali-Quintanilla, Q. Li, J.S. Vrouwenvelder, G.L. Amy, N. Ghaffour, Hybrid SBR–FO system for wastewater treatment and reuse: operation, fouling and cleaning, Desalination, 393 (2016) 31–38.
[12] R. Valladares Linares, Z. Li, V. Yangali-Quintanilla, N. Ghaffour, G. Amy, T. Leiknes, J.S. Vrouwenvelder, Life cycle cost of a hybrid forward osmosis – low pressure reverse osmosis system for seawater desalination and wastewater recovery, Water Res., 88 (2016) 225–234.
[13] T.Y. Cath, A.E. Childress, M. Elimelech, Forward osmosis: principles, applications, and recent developments, J. Membr. Sci., 281 (2006) 70–87.
[14] K. Lutchmiah, A.R.D. Verliefde, K. Roest, L.C. Rietveld, E.R. Cornelissen, Forward osmosis for application in wastewater treatment: a review, Water Res., 58 (2014) 179–197.
[15] R.C. Ong, T.-S. Chung, B.J. Helmer, J.S. de Wit, Novel cellulose esters for forward osmosis membranes, Ind. Eng. Chem. Res., 51 (2012) 16135–16145.
[16] S. Zhao, K. Huang, H. Lin, Impregnated membranes for water purification using forward osmosis, Ind. Eng. Chem. Res., 54 (2015) 12354–12366.
[17] K.Y. Wang, R.C. Ong, T.-S. Chung, Double-skinned forward osmosis membranes for reducing internal concentration polarization within the porous sublayer, Ind. Eng. Chem. Res., 49 (2010) 4824–4831.
[18] B. Mi, M. Elimelech, Organic fouling of forward osmosis membranes: Fouling reversibility and cleaning without chemical reagents, J. Membr. Sci., 348 (2010) 337–345.
[19] A. Nguyen, S. Azari, L. Zou, Coating zwitterionic amino acid l-DOPA to increase fouling resistance of forward osmosis membrane, Desalination, 312 (2013) 82–87.
[20] N.T. Hau, S.-S. Chen, N.C. Nguyen, K.Z. Huang, H.H. Ngo, W. Guo, Exploration of EDTA sodium salt as novel draw solution in forward osmosis process for dewatering of high nutrient sludge, J. Membr. Sci., 455 (2014) 305–311.
[21] L. Chekli, S. Phuntsho, H.K. Shon, S. Vigneswaran, J. Kandasamy, A. Chanan, A review of draw solutes in forward osmosis process and their use in modern applications, Desal. Wat. Treat., 43 (2012) 167–184.
[22] B.-M. Jun, T.P.N. Nguyen, S.-H. Ahn, I.-C. Kim, Y.-N. Kwon, The application of polyethyleneimine draw solution in a combined forward osmosis/nanofiltration system, J. Appl. Polym. Sci., 132 (2015) 42198–42206.
[23] J.-E. Gu, B.-M. Jun, Y.-N. Kwon, Effect of chlorination condition and permeability of chlorine species on the chlorination of a polyamide membrane, Water Res., 46 (2012) 5389–5400.
[24] Y.-N. Kwon, K. Shih, C. Tang, J.O. Leckie, Adsorption of perfluorinated compounds on thin-film composite polyamide membranes, J. Appl. Polym. Sci., 124 (2012) 1042–1049.
[25] S.P. Dubey, A.D. Dwivedi, I.-C. Kim, M. Sillanpaa, Y.-N. Kwon, C. Lee, Synthesis of graphene–carbon sphere hybrid aerogel with silver nanoparticles and its catalytic and adsorption applications, Chem. Eng. J., 244 (2014) 160–167.
[26] S.P. Dubey, A.D. Dwivedi, M. Lahtinen, C. Lee, Y.-N. Kwon, M. Sillanpaa, Protocol for development of various plants leaves extract in single-pot synthesis of metal nanoparticles, Spectrochim. Acta Part A, 103 (2013) 134–142.
[27] J.-Y. Lee, S. Qi, X. Liu, Y. Li, F. Huo, C.Y. Tang, Synthesis and characterization of silica gel–polyacrylonitrile mixed matrix forward osmosis membranes based on layer-by-layer assembly, Sep. Purif. Technol., 124 (2014) 207–216.
[28] B. Mi, M. Elimelech, Chemical and physical aspects of organic fouling of forward osmosis membranes, J. Membr. Sci., 320 (2008) 292–302.
[29] S. Lee, C. Boo, M. Elimelech, S. Hong, Comparison of fouling behavior in forward osmosis (FO) and reverse osmosis (RO), J. Membr. Sci., 365 (2010) 34–39.
[30] C. Boo, S. Lee, M. Elimelech, Z. Meng, S. Hong, Colloidal fouling in forward osmosis: role of reverse salt diffusion, J. Membr. Sci., 390–391 (2012) 277–284.
[31] Y. Kim, M. Elimelech, H.K. Shon, S. Hong, Combined organic and colloidal fouling in forward osmosis: fouling reversibility

and the role of applied pressure, J. Membr. Sci., 460 (2014) 206–212.
[32] C.Y. Tang, Q. She, W.C.L. Lay, R. Wang, A.G. Fane, Coupled effects of internal concentration polarization and fouling on flux behavior of forward osmosis membranes during humic acid filtration, J. Membr. Sci., 354 (2010) 123–133.
[33] A. Tiraferri, Y. Kang, E.P. Giannelis, M. Elimelech, Superhydrophilic thin-film composite forward osmosis membranes for organic fouling control: fouling behavior and antifouling mechanisms, Environ. Sci. Technol., 46 (2012) 11135–11144.
[34] C. Boo, M. Elimelech, S. Hong, Fouling control in a forward osmosis process integrating seawater desalination and wastewater reclamation, J. Membr. Sci., 444 (2013) 148–156.
[35] S. Romero-Vargas Castrillón, X. Lu, D.L. Shaffer, M. Elimelech, Amine enrichment and poly(ethylene glycol) (PEG) surface modification of thin-film composite forward osmosis membranes for organic fouling control, J. Membr. Sci., 450 (2014) 331–339.
[36] X. Lu, S. Romero-Vargas Castrillón, D.L. Shaffer, J. Ma, M. Elimelech, In situ surface chemical modification of thin-film composite forward osmosis membranes for enhanced organic fouling resistance, Environ. Sci. Technol., 47 (2013) 12219–12228.
[37] H.-Y. Yu, Y. Kang, Y. Liu, B. Mi, Grafting polyzwitterions onto polyamide by click chemistry and nucleophilic substitution on nitrogen: a novel approach to enhance membrane fouling resistance, J. Membr. Sci., 449 (2014) 50–57.
[38] D.L. Shaffer, H. Jaramillo, S. Romero-Vargas Castrillón, X. Lu, M. Elimelech, Post-fabrication modification of forward osmosis membranes with a poly(ethylene glycol) block copolymer for improved organic fouling resistance, J. Membr. Sci., 490 (2015) 209–219.
[39] X. Li, T. Cai, C. Chen, T.-S. Chung, Negatively charged hyperbranched polyglycerol grafted membranes for osmotic power generation from municipal wastewater, Water Res., 89 (2016) 50–58.
[40] S. Zhang, Y. Zhang, T.-S. Chung, Facile preparation of antifouling hollow fiber membranes for sustainable osmotic power generation, ACS Sustainable Chem. Eng., 4 (2016) 1154–1160.
[41] F. Liu, N.A. Hashim, Y. Liu, M.R.M. Abed, K. Li, Progress in the production and modification of PVDF membranes, J. Membr. Sci., 375 (2011) 1–27.
[42] G. Blandin, H. Vervoort, P. Le-Clech, A.R.D. Verliefde, Fouling and cleaning of high permeability forward osmosis membranes, J. Water Process Eng., 9 (2016) 161–169.
[43] R. Valladares Linares, V. Yangali-Quintanilla, Z. Li, G. Amy, NOM and TEP fouling of a forward osmosis (FO) membrane: foulant identification and cleaning, J. Membr. Sci., 421–422 (2012) 217–224.
[44] S. Yu, X. Liu, J. Liu, D. Wu, M. Liu, C. Gao, Surface modification of thin-film composite polyamide reverse osmosis membranes with thermo-responsive polymer (TRP) for improved fouling resistance and cleaning efficiency, Sep. Purif. Technol., 76 (2011) 283–291.
[45] D. Wu, X. Liu, S. Yu, M. Liu, C. Gao, Modification of aromatic polyamide thin-film composite reverse osmosis membranes by surface coating of thermo-responsive copolymers P(NIPAM-co-Am). I: Preparation and characterization, J. Membr. Sci., 352 (2010) 76–85.
[46] Q. Cheng, Y. Zheng, S. Yu, H. Zhu, X. Peng, J. Liu, J. Liu, M. Liu, C. Gao, Surface modification of a commercial thin-film composite polyamide reverse osmosis membrane through graft polymerization of N-isopropylacrylamide followed by acrylic acid, J. Membr. Sci., 447 (2013) 236–245.
[47] T.P.N. Nguyen, B.-M. Jun, J.H. Lee, Y.-N. Kwon, Comparison of integrally asymmetric and thin film composite structures for a desirable fashion of forward osmosis membranes, J. Membr. Sci., 495 (2015) 457–470.
[48] O.S. Furman, A.L. Teel, R.J. Watts, Mechanism of base activation of persulfate, Environ. Sci. Technol., 44 (2010) 6423–6428.
[49] T.P.N. Nguyen, E.-T. Yun, I.-C. Kim, Y.-N. Kwon, Preparation of cellulose triacetate/cellulose acetate (CTA/CA)-based membranes for forward osmosis, J. Membr. Sci., 433 (2013) 49–59.
[50] P.C.Y. Wong, Y.-N. Kwon, C.S. Criddle, Use of atomic force microscopy and fractal geometry to characterize the roughness of nano-, micro-, and ultrafiltration membranes, J. Membr. Sci., 340 (2009) 117–132.
[51] X. Wei, Z. Wang, Z. Zhang, J. Wang, S. Wang, Surface modification of commercial aromatic polyamide reverse osmosis membranes by graft polymerization of 3-allyl-5,5-dimethylhydantoin, J. Membr. Sci., 351 (2010) 222–233.
[52] C.Y. Tang, Y.-N. Kwon, J.O. Leckie, Probing the nano- and micro-scales of reverse osmosis membranes—a comprehensive characterization of physiochemical properties of uncoated and coated membranes by XPS, TEM, ATR-FTIR, and streaming potential measurements, J. Membr. Sci., 287 (2007) 146–156.
[53] V. Freger, J. Gilron, S. Belfer, TFC polyamide membranes modified by grafting of hydrophilic polymers: an FTIR/AFM/TEM study, J. Membr. Sci., 209 (2002) 283–292.
[54] A.R. Henn, The surface tension of water calculated from a random network model, Biophys. Chem., 105 (2003) 533–543.
[55] C.W. Extrand, Y. Kumagai, An experimental study of contact angle hysteresis, J. Colloid Interface Sci., 191 (1997) 378–383.
[56] L.-Y. Chu, Thermo-Responsive Gating Membranes: Design, Microstructures and Performances, Smart Membrane Materials and Systems, Springer Berlin Heidelberg, Berlin Heidelberg, 2011, pp. 19–68.
[57] R.J. Petersen, Composite reverse osmosis and nanofiltration membranes, J. Membr. Sci., 83 (1993) 81–150.
[58] E.M. Van Wagner, A.C. Sagle, M.M. Sharma, Y.-H. La, B.D. Freeman, Surface modification of commercial polyamide desalination membranes using poly(ethylene glycol) diglycidyl ether to enhance membrane fouling resistance, J. Membr. Sci., 367 (2011) 273–287.
[59] Y. Liu, B. Mi, Combined fouling of forward osmosis membranes: synergistic foulant interaction and direct observation of fouling layer formation, J. Membr. Sci., 407–408 (2012) 136–144.
[60] Y. Xiang, Y. Liu, B. Mi, Y. Leng, Molecular dynamics simulations of polyamide membrane, calcium alginate gel, and their interactions in aqueous solution, Langmuir, 30 (2014) 9098–9106.
[61] P. de Vos, B.J. de Haan, J.A.A.M. Kamps, M.M. Faas, T. Kitano, Zeta-potentials of alginate-PLL capsules: a predictive measure for biocompatibility?, J. Biomed. Mater. Res. Part A, 80 (2007) 813–819.
[62] M.G. Carneiro-da-Cunha, M.A. Cerqueira, B.W.S. Souza, J.A. Teixeira, A.A. Vicente, Influence of concentration, ionic strength and pH on zeta potential and mean hydrodynamic diameter of edible polysaccharide solutions envisaged for multinanolayered films production, Carbohydr. Polym., 85 (2011) 522–528.
[63] T. Matsumoto, K. Mashiko, Viscoelastic properties of alginate aqueous solutions in the presence of salts, Biopolymers, 29 (1990) 1707–1713.
[64] S. Lee, M. Elimelech, Salt cleaning of organic-fouled reverse osmosis membranes, Water Res., 41 (2007) 1134–1142.
[65] D.L. Shaffer, J.R. Werber, H. Jaramillo, S. Lin, M. Elimelech, Forward osmosis: where are we now?, Desalination, 356 (2015) 271–284.
[66] S. Mondal, S.R. Wickramasinghe, Photo-induced graft polymerization of N-isopropyl acrylamide on thin film composite membrane: produced water treatment and antifouling properties, Sep. Purif. Technol., 90 (2012) 231–238.